

Review

# Recent Studies on Thermally Conductive 3D Aerogels/Foams with the Segregated Nanofiller Framework

Mohammad Owais <sup>1,\*</sup>, Aleksei Shiverskii <sup>1</sup>, Amit Kumar Pal <sup>2</sup>, Biltu Mahato <sup>1</sup> and Sergey G. Abaimov <sup>1,\*</sup>

<sup>1</sup> Center for Petroleum Science and Engineering, Skolkovo Institute of Science and Technology, 121205 Moscow, Russia

<sup>2</sup> Center for Energy Science & Technology, Skolkovo Institute of Science and Technology, 121205 Moscow, Russia

\* Correspondence: mohammad.owais@skoltech.ru (M.O.); s.abaimov@skoltech.ru (S.G.A.)

**Abstract:** As technology advances toward ongoing circuit miniaturization and device size reduction followed by improved power density, heat dissipation is becoming a key challenge for electronic equipment. Heat accumulation can be prevented if the heat from electrical equipment is efficiently exported, ensuring a device's lifespan and dependability and preventing otherwise possible mishaps or even explosions. Hence, thermal management applications, which include altering the role of aerogels from thermally insulative to thermally conductive, have recently been a hot topic for 3D-aerogel-based thermal interface materials. To completely comprehend three-dimensional (3D) networks, we categorized and comparatively analyzed aerogels based on carbon nanomaterials, namely fibers, nanotubes, graphene, and graphene oxide, which have capabilities that may be fused with boron nitride and impregnated for better thermal performance and mechanical stability by polymers, including epoxy, cellulose, and polydimethylsiloxane (PDMS). An alternative route is presented in the comparative analysis by carbonized cellulose. As a result, the development of structurally robust and stiff thermally conductive aerogels for electronic packaging has been predicted to increase polymer thermal management capabilities. The latest trends include the self-organization of an anisotropic structure on several hierarchical levels within a 3D framework. In this study, we highlight and analyze the recent advances in 3D-structured thermally conductive aerogels, their potential impact on the next generation of electronic components based on advanced nanocomposites, and their future prospects.

**Keywords:** thermal management applications; thermal interface materials; nanocomposite aerogels; thermal conductivity; graphene; graphene oxide; boron nitride



**Citation:** Owais, M.; Shiverskii, A.; Pal, A.K.; Mahato, B.; Abaimov, S.G. Recent Studies on Thermally Conductive 3D Aerogels/Foams with the Segregated Nanofiller Framework. *Polymers* **2022**, *14*, 4796. <https://doi.org/10.3390/polym14224796>

Academic Editor: Emanoil Linul

Received: 29 August 2022

Accepted: 2 November 2022

Published: 8 November 2022

**Publisher's Note:** MDPI stays neutral with regard to jurisdictional claims in published maps and institutional affiliations.



**Copyright:** © 2022 by the authors. Licensee MDPI, Basel, Switzerland. This article is an open access article distributed under the terms and conditions of the Creative Commons Attribution (CC BY) license (<https://creativecommons.org/licenses/by/4.0/>).

## 1. Introduction

While heat dissipation is becoming a critical concern for electronic devices, technology continues to develop toward constant downsizing and higher power density. Heat accumulation can be avoided if the heat from electrical equipment is efficiently exported, such that the electronic gadget's lifetime or dependability is not compromised; otherwise, the device may cause accidents or perhaps even explode [1,2]. As a consequence, applications such as thermal management, which includes changing the role of aerogels from thermally insulative to thermally conductive, have recently been a hot topic for aerogels-based thermal management applications (TMAs) and thermal interface materials (TIMs). Polymers present ideal matrix materials due to their mechanical stability, flexibility, and high formability, but their thermal conductivity (TC) must be improved because they are thermal insulators. To do this, a highly thermally conductive filler is dispersed within the polymeric insulating matrix, to provide continuous routes through which heat can be carried across the material and then recovered or discharged. In addition, 2D nanofillers such as graphene and boron nitride have, in recent years, received a lot of interest because of their remarkable TC, which could give a significant increase in the composites' TC [2–5]. Alternative

routes include carbon nanotubes and cellulose carbonization. When fabricating such 3D structures, however, various important parameters, for 1D and 2D materials as nanofillers, must be highly considered in order to fabricate a thermally conductive functional materials for TMAs. For instance, the dimensional parameters of the flakes, the coherence of the structure, the contractual interactions between the flakes, and their purity [6].

Aerogels are perfect 3D interconnected designs with unique properties provided by tenuous networks of nanosheets or filaments; they are typically fabricated via sol–gel, freeze drying, and other phase-separating and drying techniques and possess remarkable properties, such as an extraordinarily high specific surface area, great flexibility, low density, variable tunable porosity, low dielectric constant, and low TC. Due to the above-mentioned advantageous physical features, they present a large amount of promise for applications as adaptable absorbent materials [7] and for their uses in EM shielding [8], thermal insulation [9], and wearable pressure-sensing materials [10], to be employed as a multifunctional aerogel material. The latest trends show that the modification of these low thermally conductive 3D aerogels/foams into highly thermally conductive 3D structures with excellent electrical insulation has been a popular area of discussion, specifically in the field of thermal management in the electronics industry, as thermal interface materials or phase-change materials in recent years [11–15]. At present, several types of thermally conductive 3D aerogels frameworks are being focused on, including epoxy-infiltrated or cellulose-based composite aerogels, with carbonaceous and boron nitride nanomaterials and fibrous materials being currently most widely used as fillers. However, currently and in the near future, thermally conductive 2D materials such as Mxene [16–18], transition-metal dichalcogenide (TMDC)-like molybdenum disulfide  $\text{MoS}_2$  [19,20], could play a significant role in scientific breakthroughs, as 3D structures in applications related to TMA and TIMs. For instance, numerous attempts have been made to fabricate three-dimensional (3D) graphene-based monoliths, such as aerogels with honeycomb-like structure from a 2D material, in order to meet the requirements of TIMs with both high in-plane TC and through-plane TC, which sets them apart from horizontally or vertically oriented graphene materials with high anisotropy [21–23]. As well, we observed the applications of these 2D materials as phase-change materials with the development of graphene foam or aerogel as thermal switch materials, with the transition of graphene from thermally conductive to thermal insulating [24] and with the usage of graphene aerogels as a hybrid material with metals have also been under investigation [25].

The self-assembled hierarchical 3D filler networks with porosity can be fabricated as segregated or highly segregated structures containing large backfill space/voids in the matrix system. However, due to their large porosity, 3D monoliths' TC are extremely low. Henceforth, in order to fill the porosity, pores are impregnated with thermally conductive polymers, with the aim to fill the air gaps with conductive long chains and construct thermally conductive pathways or channels inside for continuous phonon propagation and an increase in TC. Besides, this also provides higher mechanical stability without structure collapse.

## 2. Thermally Conductive 3D Aerogels Based on Carbon Nanofillers

Carbon nanofillers have sparked a lot of attention because of their unique features, including improved thermal and electrical conductivity, high mechanical strength, and ease of processing [26–29]. One viable technique for maximizing the benefits of carbon nanofillers is to segregate them into a strong three-dimensional (3D) structure for greatly improved properties relative to one-dimensional (1D) and two-dimensional (2D) structures. Such a 3D structure could now be attained by 3D frameworks/foams or aerogels-based composites or polymer-composite systems. Specific methods, such as chemical functionalization [30], orientation [31], preferential localization [32], and application of high-aspect-ratio nanofillers [33], have been developed to reduce thermal contact resistance accompanied by low filler fractions and excellent TC. Since thermal contact resistance is inversely related to contact area, filler thermal transfer efficiency should follow the rule

of  $0D < 1D < 2D < 3D$ , as the surface area grows with the filler dimensions ( $D$ ). However, achieving high TC, while maintaining excellent electrical insulation performance, remains a significant challenge for these materials, due to the high electrical conductance of the 1D and 2D nanofiller particles. This section focuses on the TCs of carbon-based 3D framework structures composed of 1D and 2D nanofillers.

### 2.1. Thermally Conductive 3D Aerogels Based on 2D Carbon Nanofillers

In recent years, the most prevalent 3D aerogels are carbon-based structures with hierarchical anisotropic architectures, where the nanofiller is segregated into a 3D framework, elements of which are made up of interconnecting nanosheets or nanofibers, often aligned or oriented. This targets unique properties such as low density, high porosity, and super elasticity [34–36]. The self-organized 3D structuring is typically created by a phase-separation process, such as freeze drying, or by other means of segregation. The 3D architecture could be created as anisotropic, if the process is directed, for example, by thermal gradient. Other methods to introduce directed self-assembly process include application of an external force field or pressure, such as a gravitational, magnetic field, or electrical field, acting in a specified direction [37,38]. The structuring is followed by the self-orientation and aligning of 2D particles at the formation of walls of the resulting 3D architecture, e.g., by surface tension, van der Waals, or other forces. The result is a sort of highly directed graphene aerogel with a hierarchical structure and specific direction. The highly aligned graphene sheets might fully leverage their high intrinsic in-plane TC, generating a highly efficient thermal conduction network, as opposed to randomly scattered graphene sheets in isotropic aerogels. For this purpose of self-assembly, several techniques such as the freeze-drying method, followed by resin impregnation, have been used in recent years for the fabrication of vertically aligned graphene-based 3D networks [36,37,39]. For example, hydrothermal reduction, aligning graphene oxide (GO) nanosheets by freeze drying, and a subsequent 2800 °C graphitization were used by Wenya and coworkers [36] to create 3D graphene networks, impregnated later with silicone rubber (Figure 1a). Instead of van der Waals forces, they assumed the nearby graphene sheets in their work were joined by chemical covalent bonding, and, using vacuum impregnation and a high-pressure treatment process, graphene was thoroughly reduced, and the defects were totally eradicated. Meanwhile, prior studies on the graphitization of graphene mainly focused on removing the oxygen-containing functional groups from graphene and the use of van der Waals forces for the connection of adjacent graphene sheets [40]. For instance, a heat treatment process was used to create vertically aligned graphene hybrid foams/epoxy composites with a high out-of-plane TC, and the effects of the graphitization were studied [40]. The application of the graphitization is a very vital step to produce high-quality graphene, as it can eliminate most of the remaining oxygen functional groups in the reduced GO unit and correct defects. Hence, by following these steps, the out-of-plane thermal conductivity of the obtained thermal interface's materials (TIMs) reached  $\sim 1.26$  W/mK, when the graphene filler concentration was only 0.5 wt.%.

Qiu et al. [37] applied the freeze-casting method to create an interconnected graphene monolith with a honeycomb-like segregated structure, mimicking cork. The structure is unique for its kind and unprecedented, with the graphene foam exhibiting good flexibility, a light weight, and good mechanical strength rather than brittleness, without the need of infiltration by a polymer. The formation procedure of the cork-like monolith by freeze casting is depicted in a graphical illustration (see Figure 1b). When a well-distributed partially reduced graphene oxide (pr-GO) dispersion freezes, pr-GO sheets are condensed at the forming ice crystals' boundaries and, subsequently, are aligned along the ice's development direction due to the squeezing action; a continuous segregated honeycomb-like network emerges, as a result. When the ice is thawed, the framework particles remain inter-connected, preserving the structure. The findings suggest that such a robust structure could pave the way for the future scientific research of segregated carbonaceous fillers, to achieve good TC and other thermal properties. At present, various carbon-based aerogels

with 2D nanofillers are being developed for numerous applications including wastewater treatment, energy storage and conversion, flame retardance, carbon dioxide capture, and catalyst supports and sensors; however, at the present time, they are now able to be employed to pertinent industrial applications, specifically related to TIMs.

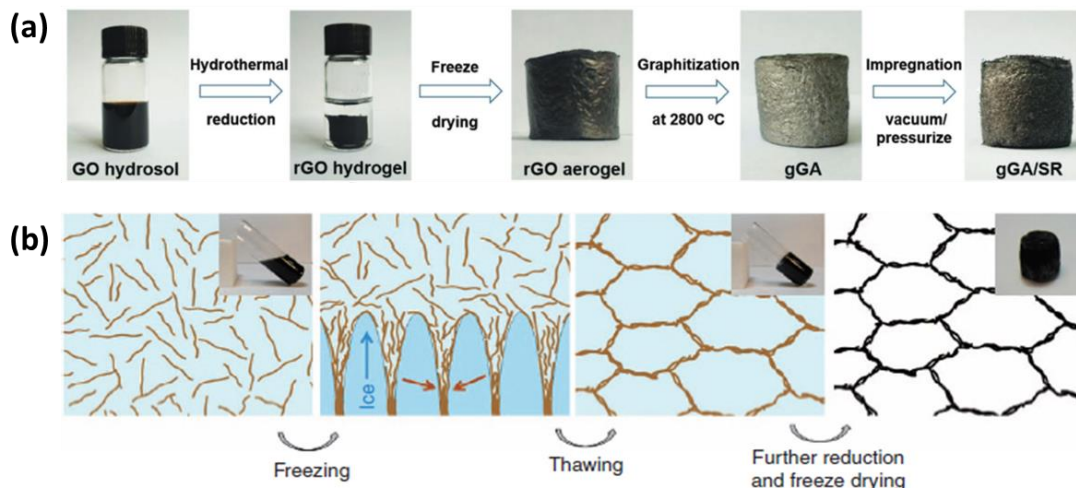


**Figure 1.** (a) Fabrication process of graphene/silicone-rubber-based thermally conductive aerogel. (Reprinted with permission from John Wiley and Sons, copyright 2019) [36]. (b) Formation of honeycomb-like structure (Reprinted with permission from nature communications, copyright 2012) [37].

Various strategies for obtaining continuous 3D networks have been proposed in the literature [41,42]. In particular, substantial study has been done on the structure of graphene aerogels, and many studies on the production and engineering of aerogels with regard to the improvement of TC can be discovered [13,15,40,43–51]. Highly thermally conductive 3D structures were subsequently infiltrated with an epoxy resin to generate polymeric nanocomposites with increased phonons transport characteristics, due to the strong connectivity of graphene planes with the chains of polymers. Weng et al., for example, used a simple process to create highly thermally conductive paths: thermal-shock exfoliation of a graphene oxide sheet, followed by the self-polymerization of silanol inside graphene frameworks (GF), was executed [52]. The self-polymerization of silanol with graphene resulted in the surface modification of graphene by the silanol group. This chemical reaction further converted silanol into siloxane, with the cross-linking of graphene frameworks with siloxane networks (SGF) with a  $-\text{Si}-\text{O}-\text{Si}-$  molecular network structure formed by self-polymerization. The GF were then compressed, and the films, with tightly packed sheets, generated a microporous honeycomb structure with pore sizes varying from several to tens of micrometers, as shown in the SEM images in Figure 2. This porous structure was made up of horizontally aligned and locally attached graphene sheets, allowing it to function as a highly anisotropic, continuous network for phonon and electron transport. The epoxy (EP) resin was then infiltrated into GF to form the EP/SGF composite. After the impregnation by epoxy, a compression procedure was used on the GF sample to eradicate the voids and create a denser structure for enhanced TC, followed by thermal curing. Siloxane molecules, which were able to immobilize the graphene sheets in the epoxy matrix system, reduced the thermal resistances in the composite with the construction of siloxane molecular bridges inside the GF structure. Thus, the in-plane and through-plane TC values of EP/SGF composites with a GF loading concentration of 20.2 wt.% reached 54.2 and 1.62 W/mK, respectively, due to improved GF quality and significantly decreased intersheet and interfacial resistances. As another important consequence of the achieved results, we can state that these aerogels' porosity can be altered, resulting in a different structural density and, consequently, in a variable amount of filler in the final 3D composite material.

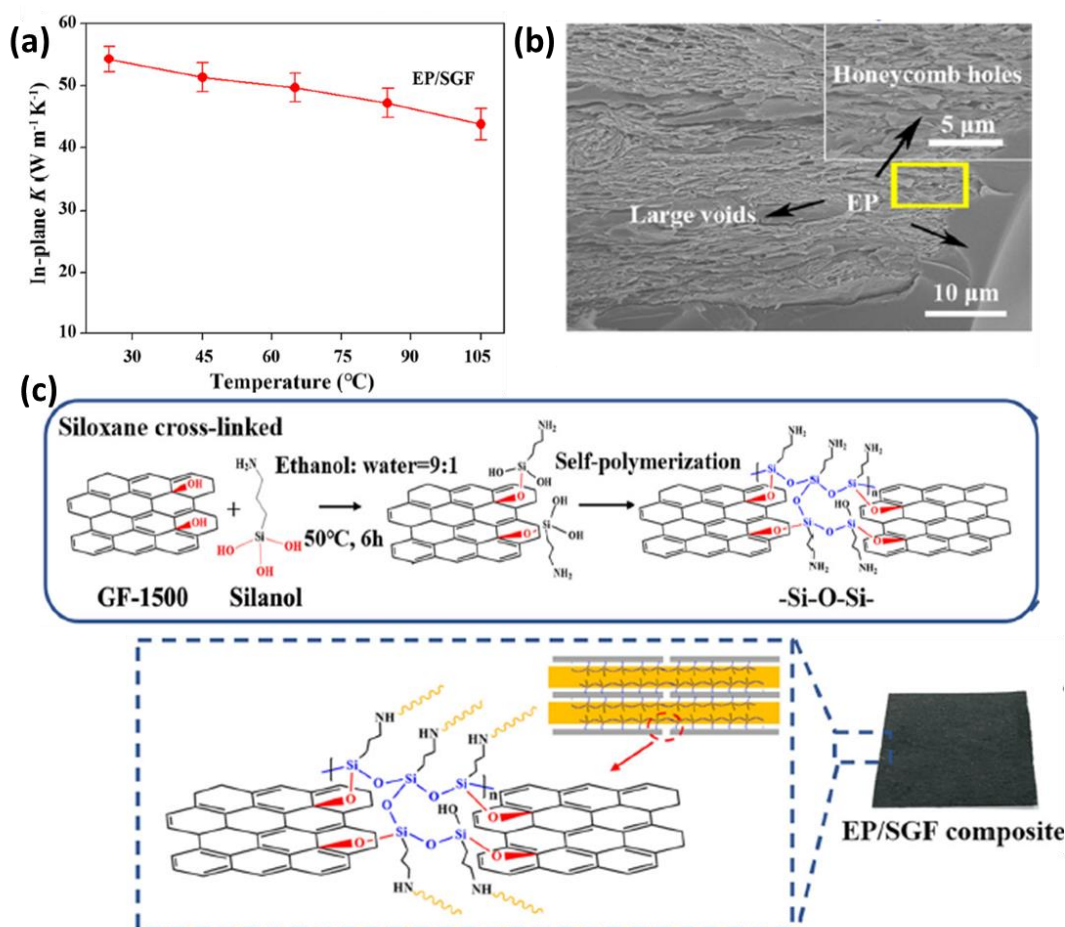


**Figure 2.** (a) In-plane thermal conductivity as a function of temperature for EP/SGF composite at a loading concentration of 20.2 wt.% graphene. (b) Cross-sectional SEM image of EP/SGF. The inset shows EP-filled honeycomb holes (Reprinted with permission from Springer, copyright 2021) [52]. (c) Schematic diagram for synthesizing EP/SGF composites.

The skeleton walls of the 3D graphene aerogels/foams used in thermally conductive polymer composites can be thought of as ultrathin graphene-based films. The quality of nanosheets and their aligned dense compaction are critical for heat conduction along the aerogel's continuous skeletons. In reality, several approaches are developed to derive graphene aerogels/foams from GO sheets, and high temperature annealing is used to eliminate the GO sheets' residual oxygen-containing groups and regenerate their lattices to heal defects in order to reduce phonon scattering [40,45,53]. However, the gases produced during the heat treatments and trapped at the skeleton walls may lead to thermally inert pores between the oriented graphene sheets, reducing the TC of the skeleton walls. For instance, Ruoff et al. used a chemical vapor deposition (CVD) technique to fabricate a three-dimensional (3D) graphene foam as the continuous thermal paths for the phase-change material. Nickel foam was employed as a template to deposit ultrathin graphite foam (UGF) with several graphene layers CVD-grown on the substrate, followed by the removal of nickel by the chemical etching process. The thin graphite hollow struts were then filled with hydrophobic paraffin wax, by immersing the foam in hot liquid wax. The fabricated composite of UGF/paraffin wax displayed the ideal phase change material, with a high TC of 3.44 W/mK at a very low graphene-loading concentration of 1.23 vol.% [54]. The TC increase can reach up to 1800%, relative to paraffin wax, as a matrix polymer with a specific TC enhancement of 1500% per 1 vol.% of graphene content. Thus, the construction of continuous graphene heat-transfer channels becomes an effective approach to improve the TCs of the polymer/graphene composite materials, due to the effective decreases in

both the contact thermal resistance among the graphene sheets and the interface thermal resistance between the graphene and polymeric matrix [50,55].

TIMs based on graphene offer a lot of potential for eliminating surplus heat created by electrical devices; however, their actual uses are frequently hampered by their poor TC, which is mostly caused by poor graphene-sheet dispersion and distribution. The TC-enhancement efficiency is still significantly below the theoretical value. The effectiveness of the 3D graphene network's TC improvements remains a significant hurdle to attain a high through-plane TC of more than 10 W/mK, with a quite low graphene-loading concentration as a filler material in a polymeric matrix. Therefore, alternative approaches are constantly being tested for their efficiency. Fei et al. studied the hydrothermal reduction of reduced graphene oxide (rGO) in the presence of high-quality graphene nanoplatelets, followed by air drying and annealing, which created vertically aligned graphene hybrid foams (GHF) with high densities [40]. The resulting vertically aligned high-quality graphene porous structure with high density, as an ideal thermal conductance network of TIMs, is extremely effective in improving the TC of its composite; when impregnated with epoxy, it attains an extremely high through-plane thermal conductivity of 35.5 W/mK at a graphene loading of 19.0 vol.% (see Figure 3). The enhancement in the TC was mainly associated with an increase in the annealing temperature, in an ascending order ranging from 1000 °C till 2800 °C. The increasing trend of temperature exhibited the removal of defects inside the graphene structure, as observed in the Raman mapping and XPS spectrum, resulting in a higher TC. Raw (not annealed) GHF5 (the 5 comes from the mass ratio of graphene oxide:graphene = 1:5) and its thermally annealed equivalent GHF-2800 (GHF annealed at 2800 °C) are characterized using ID/IG Raman mapping (Figure 3b,d, respectively). A large blue region surrounds the yellow and green sections in GHF5 (Figure 3b). The blue regions correspond to high-quality GNPs with an ID/IG value of less than 0.2, whereas the yellow and green regions, which have larger ID/IG values >0.5, are caused by rGO sheets with residual oxygen functional groups and defects. GNPs are interconnected by rGO sheets, according to this ID/IG distribution. The Raman mapping of GHF-2800, a GHF annealed at 2800 °C, is full of dark blue (Figure 3d), and most ID/IG values remain below 0.025, because this temperature is high enough to entirely eliminate the leftover oxygen functional groups and repair the lattice defects. In support of these findings, XPS spectrum (Figure 3e) shows a decrease in the oxygen content, with a complete reduction in the oxygen peaks for GHF-2800. Hence, augmentation in TC of polymer composites can be directly linked to the annealing temperatures of their graphene structures for the removal of phonon-scattering defects and decreasing contact thermal resistance. The annealed graphene hybrid-foams-based epoxy composites are, thus, well-suited for TMA due to their outstanding TC characteristics, especially when the annealing is conducted at extremely high or ultrahigh temperatures, as supported by several authors [56,57]. Typically, graphene porous structures are made up of chemically or thermally reduced graphene sheets, which often have residual oxygen-containing groups and lattice defects that can produce phonon scattering [58]. The high-temperature annealing process, fortunately, has been shown to be effective in eliminating these functional groups and repairing the defects. For illustration, the preparation of thermally annealed defect-free graphene sheets was reported by Lian et al. [59], in which phonon-scattering centers and defects were greatly minimized, for the effective thermal transport of phonons by high temperature annealing, at around 2200 °C for thermally conductive phase-change materials, which displayed a high TC of 3.55 W/mK at a 10 wt.% of graphene-loading concentration. Similarly, in support of the aforementioned statements, Gao et al. employed a high-temperature annealing and mechanical pressing to create a high-quality graphene sheet with an ultrahigh TC of approximately 1940 W/mK and good flexibility for high-power electronic devices [60].

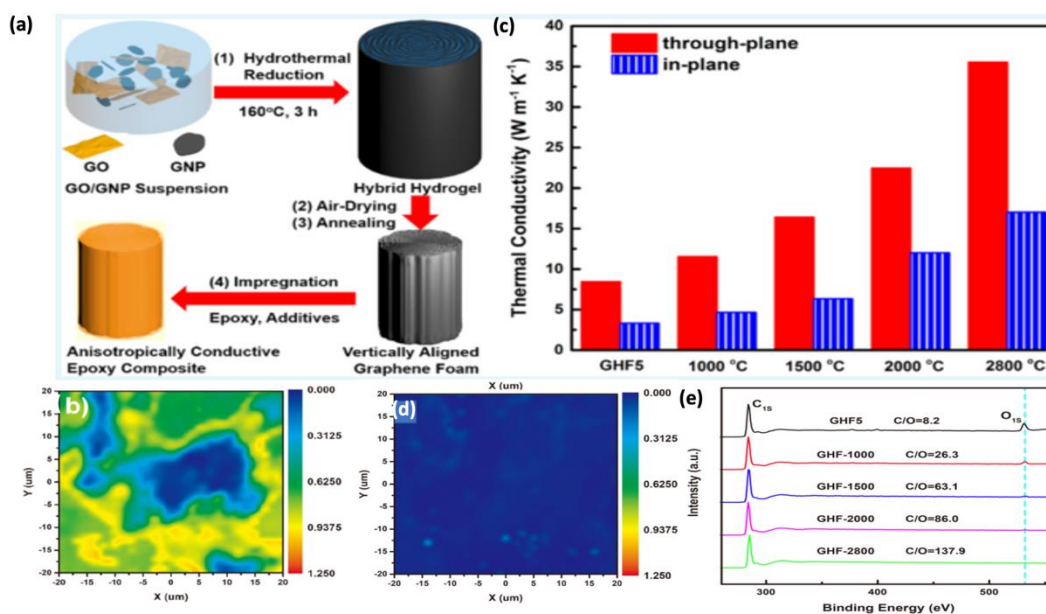


**Figure 3.** (a) Schematic illustration of the fabrication process: (1) vertically aligned reduced graphene oxide (RGO)/graphene nanoplatelets (GNP) hybrid hydrogels by hydrothermal process, (2) air-dried vertically aligned graphene hybrid form (GHF), (3) thermally annealed GHF, and (4) its epoxy composite. (b) Raman  $I_D/I_G$  mapping of GHF5 (graphene oxide:graphene = 1:5) neat hybrid filler. (c) Effect of thermal annealing on the thermal conductivity of epoxy graphene hybrid foam composites conducted at various high temperatures. (d) Raman  $I_D/I_G$  mapping of GHF-2800 (annealing at 2800 °C). (e) XPS spectra of annealed GHFs at different temperatures. (Reprinted with permission from American Chemical Society, copyright 2018) [40].

Most carbon-based aerogels have high intrinsic electrical conductivities, limiting their usage in electronic packaging materials' systems due to issues such as short circuiting and other complications. As a result, converting carbon-based aerogels from electrically conductive to electrically insulating, while maintaining their outstanding mechanical and thermal qualities, may prove to be highly desirable and essential. Developing such carbon-based aerogels with a high electrical resistivity and heat dissipation capability, as well as strong structural stability, is now a major issue. Among several developed approaches, the nanohybridization of thermally conductive boron nitride with synergy with carbon-based materials such as graphene, graphene oxide, and reduced graphene oxide seems to be one of the most promising solutions to solve this problem [61–63]. For instance, the fabrication of 3D hybrid boron nitride graphene oxide nanosheets as aerogels with epoxy impregnation was explored, and the results showed an excellent TC of 4.53 W/mK (11.6 vol.% loading fraction) and good electrical insulation, with electrical conductivity reaching a low scale of  $10^{-11}$  S/m, almost equaling the electrical conductivity of pure epoxy [63]. Moreover, for another different approach [13], a hydrothermal procedure aided by hydrofluoric acid produced highly compressible and thermally conductive, though electrically insulating, fluorinated graphene aerogels (FGAs). The introduction of fluorine to fluorinated graphene aerogels via the hydrothermal process results in a substantial reduction in charge-carrier density and changes the band gap of the inherent graphene. These aerogels have been shown to be very insulating, with the lowest electrical conductivity measured at  $4 \times 10^{-9}$  S/m, with the tunable band gap as reported in this work [13], which allows for the modification of their electrical insulating performance. Moreover, the electrical resistance of these FGAs varies depending on the deformation condition.

## 2.2. Thermally Conductive 3D Aerogels Based on 1D Carbon Nanofillers

Carbon nanotubes (CNTs) have been reported extensively for their usage as 1D carbon materials for 3D-based frameworks. Since their first discovery more than three decades

ago, CNTs have drawn a lot of attention due to their exceptional physical, thermal, and mechanical properties [10,64,65]. In order to improve materials' performance, CNTs are used as nanofillers in polymeric materials, such as epoxy resin, polyimide, and poly (methyl methacrylate), for achieving high TC. Due to their inherent high TC, of around 6600 W/mK (via MD simulation) and ~3000 W/mK (experimentally) [66], CNTs exhibit a vital role in TIMs for the dissipation of heat energy in electronic devices, with important factors including alignment/orientation, loading percentages, dispersion, density, aspect ratio, presence of topological and inherent structural defects, and chemical interaction of polymer matrix materials with CNTs [67,68]. In the case of a 3D framework aerogel structure [2,26], vertically aligned carbon nanotubes (VACNTs) are an ideal material for achieving a high TC with good mechanical characteristics [69]. By improving the contact at the interface or densifying the CNTs, the thermal interface resistance is decreased, resulting in an increased TC. Moreover, the heat transport can also be improved immensely by using high-temperature annealing to reduce defect density [70], utilizing mechanical densification to increase the volume percentage of CNTs [71], and enhancing the CNT alignment through processing with strong magnetic fields [72]. In thermally conductive aerogels with a polymer matrix, CNTs work in synergy with other carbon fillers to create a hybrid filler composite [65,73]. For instance, a unique class of paraffin-based shape-stable phase-change materials was fabricated by vacuum-assisted impregnation of paraffin into an aerogel comprised of reduced graphene oxide (rGO) and carbon nanotubes (CNTs). Investigations were done into how the morphology, structure, and properties of the paraffin composite were affected by the ratio of rGO to CNTs in the 3D-network structure. The 3D-network topology of rGO/CNTs possessed a high TC and acted as a single thermally conductive skeleton with good stability.

Other than carbon nanotubes, carbon fibers have been used as 1D fillers in 3D polymer composites for TMAs [74–78]. These carbon fiber composites are typically fabricated by the combination of several steps, including carbonization, graphitization, and high-temperature hot-press molding techniques, and possess high TCs in both the axial and radial directions, with in-plane TC exceeding 900 W/mK [79,80]. Little work has been done on the thermally conductive 3D-based aerogels based on carbon fibers, but, nevertheless, 3D-based fabricated structures of 1D carbon fiber have been reported with increased interest, in recent years. For instance, in their experimental study, Yao et al. first created porous carbon-fiber (C/C) composites using low-temperature hot-press molding [81]. Following that, a chemical vapor infiltration (CVI) technique, precursor impregnation, and pyrolysis were used to densify the porous C/C composites. Finally, carbon bulks with a density of 1.90 g cm<sup>3</sup> and in-plane TC of 667 W/mK were produced, following the graphitization process at 3000 °C. Similarly, in a study conducted by Zhang et al., the researchers densified large-diameter graphite fiber bundles and developed a method to synthesize two types of carbon rods without the use of hot pressing [74]. One kind was fabricated by injecting phenolic resin into the bundles of carbon fiber, followed by curing, carbonization, graphitization, and densification with a CVI technique, while another type was created by subjecting the carbon bundles to CVI treatment, with further densification of both types of carbon rods finally. After graphitization, these kinds of carbon rods achieved TCs of around 569 and 675 W/mK, respectively. Moreover, in another study conducted by Nan Sheng et al., the role of wrapped graphene on the vertically aligned hollow carbon fiber was investigated with impregnation by Paraffin wax [78]. Biomass cotton was used to fabricate porous carbon scaffolds as the supporting framework for creating high-performance phase-change materials (PCMs), in order to address the issues of the leakage and poor heat conductivity of the composite materials based on paraffin (Figure 4). The phase-change composite (PCC) with an 8.5 wt% filler concentration demonstrated a high TC along the axial fiber direction of 2.68 W/mK, which is 10 times greater than that of paraffin. The segregated carbon fibers are connected by the porous carbon frameworks produced by the introduction of urea, which are tightly coiled around the fibers and filled in where there are gaps. Hollow carbon fibers and porous graphene frameworks are part of a three-dimensionally connected and crosslinked

carbon network that can provide various, continuous pathways for the thermal-conduction phenomenon. Particularly, the high TC of graphene type carbon is projected to significantly improve the PCC's ability to conduct heat and to be used in applications related to TMA.

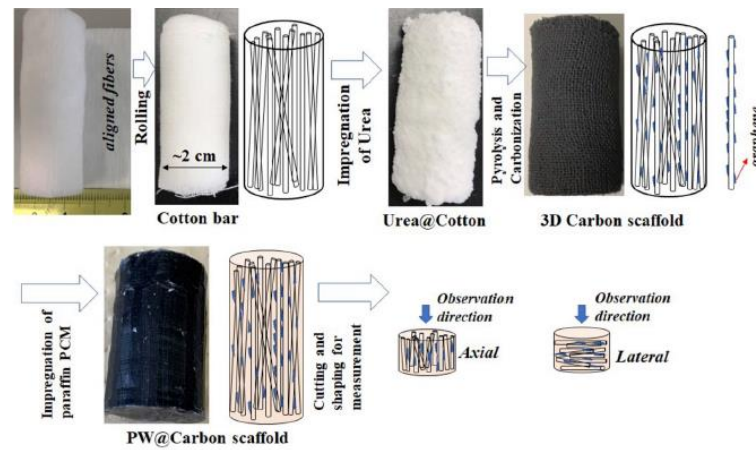


**Figure 4.** Schematic for the fabrication of 3D carbon-fiber-wrapped graphene phase-change composite (Reprinted with permission from Elsevier, copyright 2022) [78].

**Table 1.** Thermal conductivities of various aerogels 3D frameworks, as mentioned in the literature.

Polymer Matrix	Filler Loading	Type of 3D Structure	Thermal Conductivity, W/mK (Through-Plane)	Thermal Conductivity, W/mK (In-Plane)	Technique for Measuring Thermal Conductivity	References
Epoxy	25.4 vol.% graphene/boron nitride	Graphene/boron nitride aerogel	11.01	5.9	Laser flash	[61]
Epoxy	2.5 vol.% graphene	Graphene aerogel	9.1	3.6	Laser flash	[61]
Epoxy	19.0 vol.% graphene oxide/graphene nanoplatelets	Vertically aligned graphene hybrid foam	35.5	17	Laser flash	[40]
Polydimethylsilo-xane (PDMM)	11.62 wt.% graphene	Graphene foam	1.62	28.77	Laser flash	[50]
Epoxy	0.75 vol.% graphene	Graphene aerogel	6.57	1.1	Laser flash	[49]
Epoxy	2.30 vol.% graphene	Polyamic acid salt/graphene oxide (PAAS/GO) hybrid aerogels	20	17	Laser flash	[48]
—	Density of graphene aerogel 150.49 mg cm <sup>-3</sup>	Graphene aerogels films	0.7	53.56	Laser flash	[47]
Paraffin wax	—	Polyamic acid/graphene oxide aerogel	2.68	8.87	Laser flash	[46]
—	5 wt.% graphene	Graphene aerogels	—	4.28	Laser flash	[45]
Epoxy	7.2 wt.% (6.0–1.2 wt% copper-graphene)	Copper nanowires/graphene aerogels	—	0.51	Hot disk	[44]

Table 1. Cont.

Polymer Matrix	Filler Loading	Type of 3D Structure	Thermal Conductivity, W/mK (Through-Plane)	Thermal Conductivity, W/mK (In-Plane)	Technique for Measuring Thermal Conductivity	References
Epoxy	—	Fluorinated graphene aerogel	—	2.5	Steady-state method	[13]
—	100 wt.% boron nitride nanosheets	Boron nitride aerogels	—	25.2	—	[82]
Polyethylene glycol	—	Boron nitride aerogels	—	0.67	Laser flash	[83]
Poly vinyl alcohol	0.12 wt.% boron nitride nanosheets	Boron nitride/polyvinyl alcohol hydrogels	—	0.68	Transient plane source method	[84]
Poly vinyl alcohol	67.7 wt.% boron nitride	Boron nitride/polyvinyl alcohol aerogels	1.1	10.04	Laser flash	[85]
Cellulose nanofiber	50% wt.% boron nitride	Boron nitride (BN)/cellulose nanofiber aerogels	—	2.71	Laser flash	[1]
Polydimethylsiloxane (PDMS)	3.32 wt.% reduced graphene oxide (rGO)-cellulose	Reduced graphene oxide (rGO)/cellulose polydimethylsiloxane	—	0.65	Laser flash	[86]
Cellulose	33wt.% boron nitride/cellulose	Boron nitride–nanosheet/cellulose nanofiber aerogel	—	0.57	Hot wire transient method	[87]
Epoxy	34 vol.% boron nitride	3D boron nitride aerogel/epoxy	—	4.42	Laser flash	[88]
Epoxy	9.6 wt.% boron nitride	3D carbonized cellulose aerogel/epoxy	—	2.11	Hot disk	[89]
Paraffin wax	1.23 vol.% graphene	Ultrathin graphite foams	—	3.44	Steady-state method	[54]
Epoxy	1.0 wt.% MXene (Ti <sub>3</sub> C <sub>2</sub> )	MXene (Ti <sub>3</sub> C <sub>2</sub> )/epoxy	—	0.587	Laser flash	[17]
Polydimethylsiloxane (PDMS)	25.4 wt.% boron nitride	Boron nitride/PDMS	—	1.5	Laser flash	[90]
Polyvinyl alcohol	66 wt.% boron nitride	BN/PVA aerogel cake composite	0.61	0.76	Laser optical thermal scanner	[38]

### 3. Cellulose Based Thermally Conductive Aerogels

Cellulose, with an intrinsic TC that is  $\sim 0.04$  W/mK, is a biologically friendly compound that is rich in oxygen and hydroxyl functional groups, which shows good compatibility with most of the 2D-based nanofillers, for the formation of thermally conductive aerogels [86,87,89]. One such thermally conductive fillers utilized in cellulose-based composites is boron nitride (BN) (also known as white graphene) [91]. BN can be exfoliated into boron nitride nanosheets (BNNS), which are 2D nanosheet structures with strong thermal conductance characteristics [92,93]. BNNs, featuring a graphene-like crystal structure, not only offer outstanding mechanical stability and thermal conductivity ( $\sim 600$ – $2000$  W/mK) but also have low coefficient of thermal expansion, good electrical insulation, antioxidative properties, and thermal stability [94–96].

The development of a 3D-interconnected network structure based on BNNs can improve the thermal transfer efficiency per unit mass, i.e., TC, for lightweight, portable electronic equipment. This material can be employed in 3D aerogels for a variety of applications, including insulation and fire protection, as a host for polymer matrix composites, and so on. In order to enhance the TC of BN aerogels, Wang et al. [86] fabricated boron nitride (BN)/cellulose nanofiber (CNF) composite structures. They varied and adjusted

the BNNs content in the CNF and made nanopaper using two methods: simple blending and the aerogel 3D-skeleton approach. The aerogel-based nanopaper had 93.1% better TC ( $2.71 \text{ W/mK}$ ) than the blended nanopaper ( $1.44 \text{ W/mK}$ ) with 50 wt% BNNs loading, as shown in Figure 5a. The higher TC of the aerogels could be owing to the BN nanosheets spreading more evenly and uniformly inside the cellulose matrix compared to the paper-blending process. Furthermore, compressing the porous aerogels reduces the amount of trapped air bubbles/pores, allowing the boron nitride nanosheet contacts to be closer together, for better phonon transfer inside the composite system. The volume electrical resistivity of the BNNs/CNF nanopaper ( $3.8 \times 10^{14} \Omega \text{ cm}$ ) (Figure 5d) was also found to be higher than that of pure CNF ( $2.6 \times 10^{14} \Omega \text{ cm}$ ), which is still much higher than the insulation requirement (electrical resistivity  $> 10^9 \Omega \text{ cm}$ ) [97]. Besides, the aerogels demonstrated qualities such as high strength, low thermal expansion coefficient, and environmental friendliness.

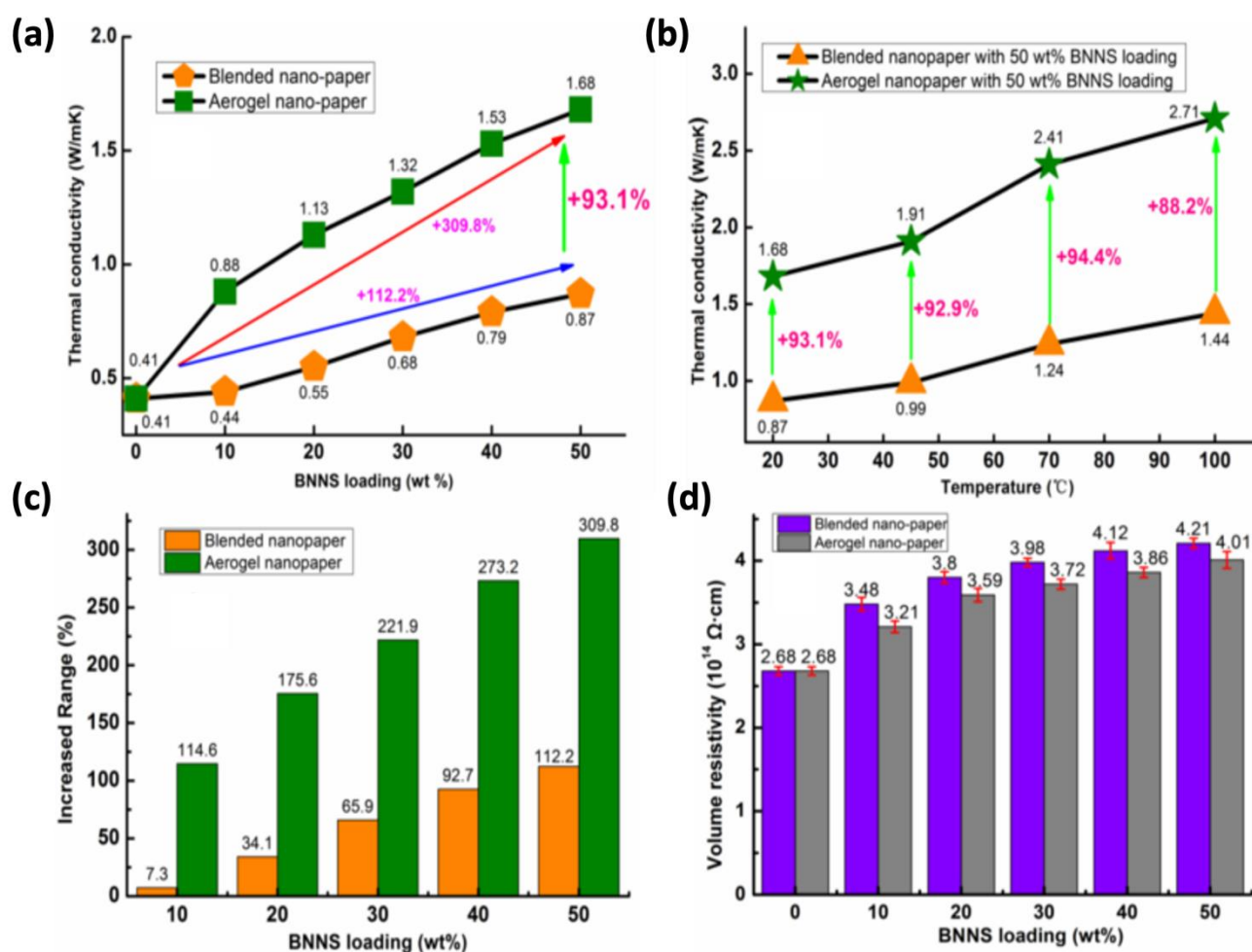


**Figure 5.** Blended nanopaper vs. aerogel nanopaper: (a) thermal conductivities with different BN loading content; (b) thermal conductivities at elevated temperatures with BN loading content of 50wt.%; (c) aerogels' composite enhancement factor; (d) electrical volume resistivity [1].

The 3D aerogels synthesized from hydroxyl functionalized boron nitride nanosheets (BNNs) via the freeze-casting method can have a high TC over a wide temperature range. As the temperature tends to increase from  $30 \text{ }^\circ\text{C}$  to  $300 \text{ }^\circ\text{C}$ , the in-plane TC of functionalized BN-polyimide (FBN-PI) aerogels with 50 wt.% filler loading increases from  $6.7 \text{ W/mK}$  to  $9.8 \text{ W/mK}$ , with an ultralow density of  $6.5 \text{ mg/cm}^3$ , as shown in Figure 6a [98]. This enhanced TC is highly suited for high temperature TMA, especially as a lightweight thermal conductor.

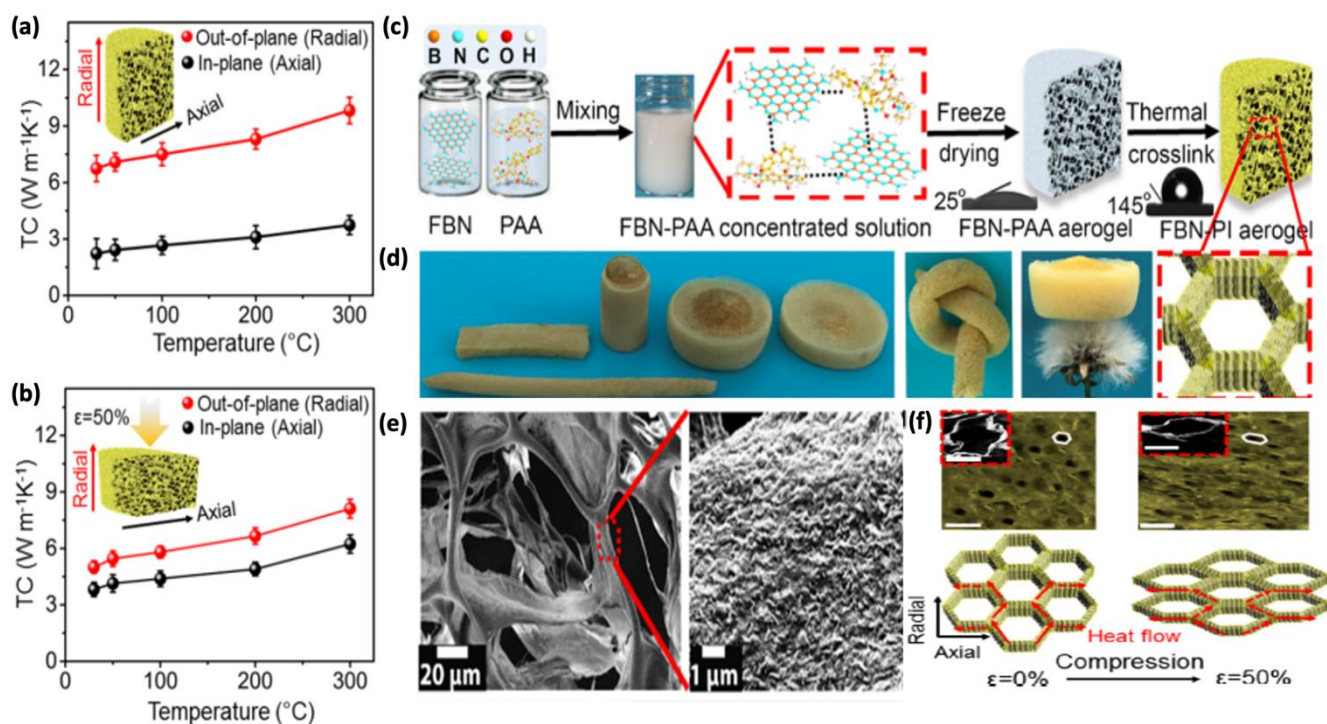


**Figure 6.** Thermal performances of aerogels: (a) thermal conductivities of FBN-PI aerogel without compression at different temperatures; (b) thermal conductivities of FBN-PI aerogel with 50% compression at different temperatures; (c) schematic illustration of the fabrication process of FBN-PI aerogel; (d) digital photographs of FBN-PI aerogels with different shapes, under knot, and floating on the flower stamen; (e) SEM and TEM images with different magnification of FBN-PI aerogels; (f) optical microscope images ( $200 \mu m$ ) and SEM images ( $50 \mu m$ ) of FBN-PI-2 aerogel from 0% strain to 50% strain and corresponding anisotropic thermal conduction mechanism [98]. (Reprinted with permission from American Chemical Society, copyright 2019).

In the condition where the same aerogel is compressed, the TC increases only moderately as the temperature rises. Despite Umklapp phonon-scattering, this phenomenon results from the rising gas' thermal radiation at elevating temperatures. Under compression, the out-of-plane TC decreases significantly, while the in-plane TC rises, owing to a change in the anisotropic cellular honeycomb structure, with increased axial heat transfer extension with stretched boron nitride bonds (see Figure 6f). Furthermore, after compression, the reduced air gaps between the layers aid in the improvement of the in-plane TC. The honeycomb cell is elongated parallel to the radial direction (out-of-plane) under a compression deformation of around 50%, resembling the layer-by-layer structure. As a result of this, the in-plane TC increases, while the out-of-plane TC decreases, causing the TC to shift from thermal anisotropy toward isotropy. As a result, it is possible that the elastic thermal anisotropic property of the FBN-PI aerogel could be used for thermal-based strain sensors, and, furthermore, this proves that BNNs-based aerogels may be used to manage thermal energy even at high temperatures.

It is not necessarily required to create 3D-framework filler/polymer in one manufacturing step; a polymer framework can be filled with filler material afterward, providing suitable thermal properties. In one of the findings reported recently, reduced graphene oxide (rGO)/cellulose-based aerogels were fabricated via a two-stage freeze drying and self-assembly technique, where first the structure of the cellulose aerogels (CA) was formed, followed by a second step, freeze drying it immersed in GO as a filler mixture [86]. The mechanism includes the gradual wrapping of rGO on cellulose fibers, for the formation of a 3D double-layered thermally conductive network with a skin-core-type structure. After annealing, the single nanofibers of carbon cellulose aerogels (CCA) have a twisted-like

structure and are around 6  $\mu\text{m}$  in diameter, which is mostly due to the removal of oxygen-containing functional groups and the carbonization of the cellulose (see Figure 7c–e). The annealing of aerogels was executed, followed by infiltration with polydimethylsiloxane (PDMS) via the vacuum impregnation technique, to form the final composite. The skin-core structure of CCA@rGO is substantially conserved after backfilling with PDMS, and the 3D double-layered thermally conductive network structure of CCA@rGO is not considerably degraded, with the PDMS disseminated more uniformly in the gaps of the 3D thermally conductive network of CCA@rGO. As a result, the composite exhibited enhanced thermal conductivity of 0.65 W/mK, with an excellent electromagnetic shielding effect.

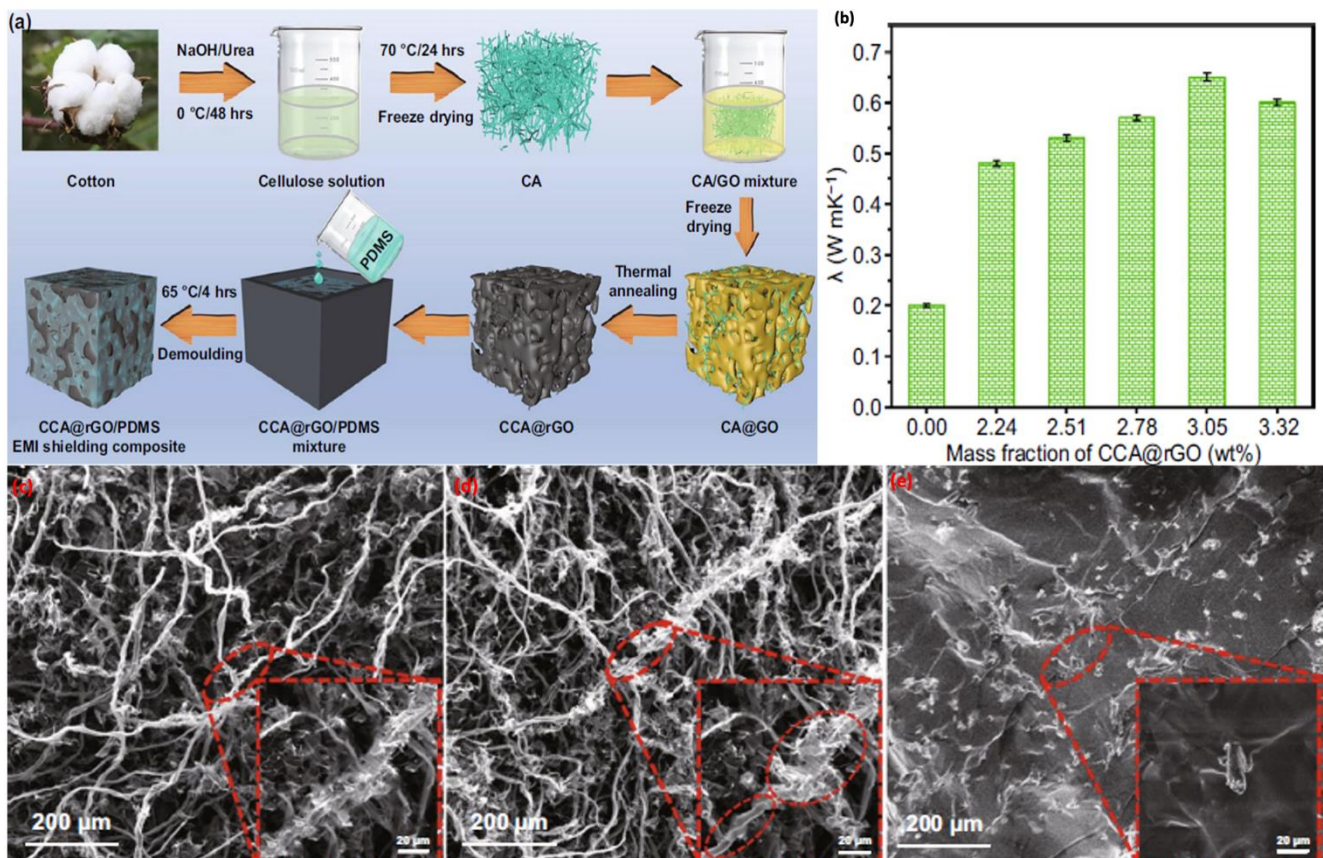


**Figure 7.** (a) Schematic illustration of the fabrication procedure for rGO-cellulose/PDMS aerogels; (b) thermal conductivity of rGO-cellulose/PDMS aerogels composites with various filler loading of rGO-cellulose in PDMS as matrix [86]; (c) SEM images of CA; (d) CCA; (e) CCA@rGO-based PDMS composites.

#### Biomass-Based Carbonized Cellulose Thermally Conductive Aerogels

Due to their abundance of supplies, affordability, environmental friendliness, and naturally porous nature, biomass materials are widely desired for solar applications. One of the most alluring ways to increase the stability and effectiveness of solar energy is to use energy-storage strategies based on organic composite with a high TC and strong shape stability. With the improvement of the TC and shape stability of organic composites, they are reported to be achievable through the creation of three-dimensional heat transfer scaffolds [99]. For this purpose, cellulose-based carbonized aerogels are employed [100–102]. Wu et al. reported a biomass-carbonized aerogel with a TC of 1.17 W/mK, where cellulose was selected as a precursor for the carbon source [101]. Techniques involving immersion expansion, orientation, freeze-drying, and carbonization methods were tested to create 3D cellulose-based carbon aerogels. After carbonization, the procedure involved the impregnation of various volume and weight percentage concentrations of stearic acid/graphene

mixtures, by vacuuming them for more than 12 h to completely remove the trapped air bubbles (Figure 8). The aerogel exhibited a high specific surface and productivity as well as minimal structural shrinkage, when tert-butanol/deionized water was used as the cosolvent. The use of graphene and a 3D-directed graphitized porous network ensured good broadband absorption, effective heat transport, and efficient thermal storage.

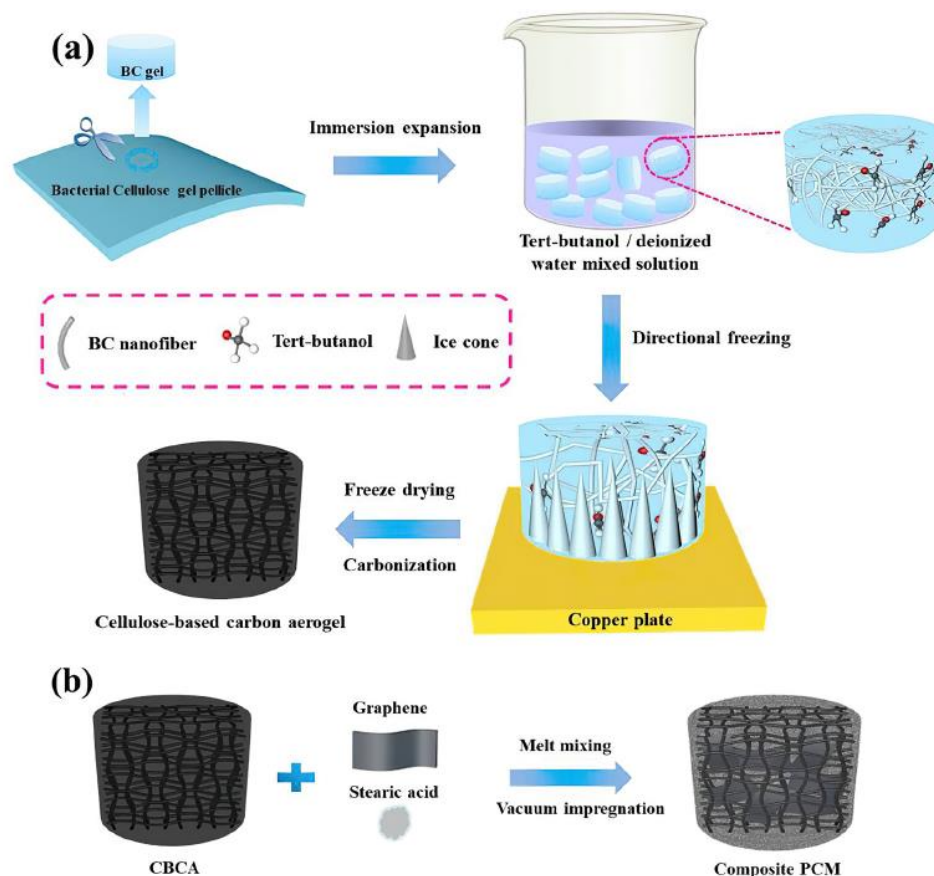


**Figure 8.** Schematics of the fabrication of: (a) cellulose-based biomass carbon aerogel preparation and; (b) composite phase-change material. (Reprinted with permission from Elsevier, copyright 2022) [101].

#### 4. Carbon Nanomaterial-Based In Situ Construction of Thermally Conductive 3D Frameworks with Polymers

The ability of polymers to transmit heat must be improved by the creation of an interconnected network. Adding prefabricated 3D networks as fillers is a successful way to create continuous heat conduction networks in polymer matrices. However, other approaches, including adding a higher weight percentage of particle fillers, are less effective, as they deteriorate the mechanical integrity of thermally conductive polymer composites. However, the in-situ fabrication of a connected conducting composite network is another easy and scalable method that has been reported in recent years for fabricating thermally conductive 3D-framework polymer composites [103–105]. In this procedure, following the fabrication of carbon nanomaterial-based polymer composites, polymer powders are first precoated with a thermally conductive filler before being hot-pressed and compressed into a monolith framework. For instance, graphene/polymer composites were fabricated by Lin's group, by coating graphene on polymer powder first, then drying and hot-pressing it to form a 3D scaffold structure [106]. In light of this, a continuous graphene-conducting polymer matrix network is established, and this method can be employed with most of the thermoplastic polymers, including polyethylene, polypropylene (PP), polyvinyl alcohol (PVA), and polyvinylidene. Hence, as shown in Figure 9, the TC of PP composites

with graphene network connections, built in situ, was far more substantial than those of composite materials with randomly displaced/positioned graphene in a PP polymer. Using this similar method, Wang's team fabricated and developed a highly organized 3D CNTs/polystyrene composites framework for a high TC [107]. After compression and heat-treatment processes, a 3D CNT interconnected structure was created in the polystyrene matrix by coating the polystyrene (PS) particles with MWCNTs. With the help of this procedure, distinctive composite structures with superior properties were formed, and the composites displayed a continuous phase structure of the PS phase and MWCNT network by incorporating an intact, uniform, and well-defined 3D network of MWCNTs.

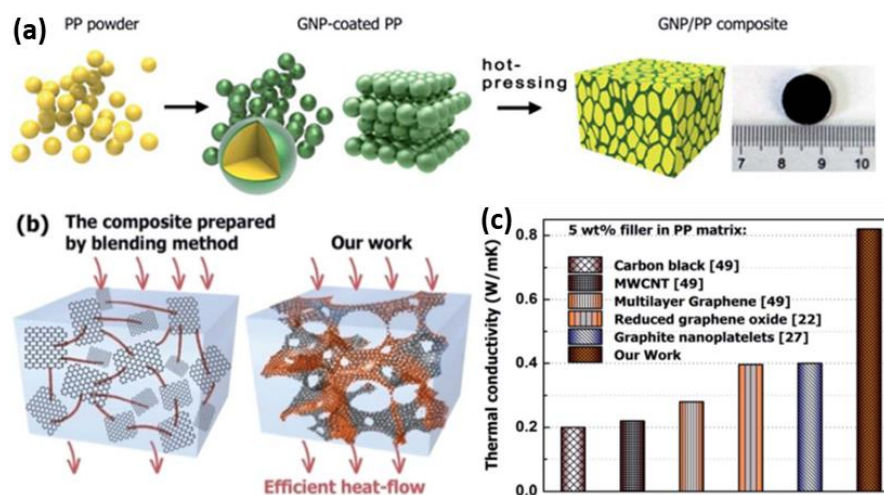


**Figure 9.** Schematics of the fabrication process of GNP/PP framework composites. (a) Fabrication of GNP-coated / PP composites; (b) Diagram comparing effective thermal conduction through a network of connected graphene to that through dispersed graphene; (c) Comparison between the TC values of these composites and randomly dispersed filler composites with the TC of GNP/PP composites (Reprinted with permission from Royal Society of Chemistry, copyright 2017) [106].

Apart from such benefits, however, this strategy has a number of drawbacks. First, only thermoplastic polymer materials may be prepared using this thermoforming technique, so it is frequently necessary to process the polymer into tiny particles beforehand [106]. Second, the formation of an anisotropic, thermally conductive networks composite is a serious challenge with this technique, as it favors the formation of isotropic networks with a comparatively low TC, with respect to the high TC reported in recent years. As a result, the applicability of this in situ construction method for 3D interconnected conducting network is limited.

Table 1 shows the thermal conductivities of various 3D aerogels, with the reference to the testing procedure involved. It demonstrates the significant quantity of study being conducted globally to determine the thermal conductivities of 3D aerogels frameworks.

## 5. Conclusions

This brief study provides an overview of the literature on the thermally conductive three-dimensional frameworks that have been developed in recent years, for their use in thermal management applications. We expect that, in the near future, these thermally conductive frameworks will yield some significant findings for their applications in thermal management, particularly as thermal interface materials, phase-change materials, and thermally conductive structures such as aerogels/foams/sponges, which are expected to reshape the electronics industry. Most researchers have been working on constructing highly porous 3D-skeleton structures, with aligned thermally conductive fillers such as graphene and boron nitride, in recent years. These porous microstructures aided in the infiltration and intercalation of the inserted polymer chains, for the bridging effect of an effective phonon transfer, resulting in the increased thermal conductivity of the whole 3D

framework. Furthermore, the filler thermal transfer efficiency of 3D structures results in a larger effective contact area with the impregnating polymer chains, lowering the composite system's thermal resistance. Further investigation into thermally conductive 3D structures could be very promising in the electronics sector, since it could lead to the development of low-cost, highly thermally conductive components that are easier to fabricate and scale up than conventional phase-change and thermal interface materials. The high electrical insulative properties accompanying the desired thermal conductivity values present a challenge, even nowadays, highlighting one of the trends for future endeavors.

**Author Contributions:** Conceptualization, Formal analysis, Investigation, Writing part—original draft, Writing—review and editing, M.O.; Visualization, A.S.; Validation, A.K.P.; Review, B.M.; Conceptualization, Resources, Review and editing, Supervision, Project administration, S.G.A. Funding acquisition. All authors have read and agreed to the published version of the manuscript.

**Funding:** This research received no external funding.

**Conflicts of Interest:** The authors declare no conflict to interest.

## References

1. Wang, X.; Yu, Z.; Bian, H.; Wu, W.; Xiao, H.; Dai, H. Thermally conductive and electrical insulation BNNS/CNF aerogel nano-paper. *Polymers* **2019**, *11*, 660. [[CrossRef](#)] [[PubMed](#)]
2. Owais, M.; Javed, M.H.; Akram, M.Z.; Paxton, W.F.; Akhatov, I.S.; Abaimov, S.G. Review—Recent Advances in Thermally Conductive Paper-Like Films. *ECS J. Solid State Sci. Technol.* **2021**, *10*, 033001. [[CrossRef](#)]
3. Lee, C.; Wei, X.; Kysar, J.W.; Hone, J. Measurement of the elastic properties and intrinsic strength of monolayer graphene. *Science* **2008**, *321*, 385–388. [[CrossRef](#)] [[PubMed](#)]
4. Balandin, A.A.; Ghosh, S.; Bao, W.; Calizo, I.; Teweldebrhan, D.; Miao, F.; Lau, C.N. Superior thermal conductivity of single-layer graphene. *Nano Lett.* **2008**, *8*, 902–907. [[CrossRef](#)]
5. Owais, M.; Zhao, J.; Imani, A.; Wang, G.; Zhang, H.; Zhang, Z. Synergetic effect of hybrid fillers of boron nitride, graphene nanoplatelets, and short carbon fibers for enhanced thermal conductivity and electrical resistivity of epoxy nanocomposites. *Compos. Part A Appl. Sci. Manuf.* **2019**, *117*, 11–22. [[CrossRef](#)]
6. Zhang, F.; Feng, Y.; Feng, W. Three-dimensional interconnected networks for thermally conductive polymer composites: Design, preparation, properties, and mechanisms. *Mater. Sci. Eng. R Rep.* **2020**, *142*, 100580. [[CrossRef](#)]
7. Li, C.; Li, Z.; Qi, X.; Gong, X.; Chen, Y.; Peng, Q.; Deng, C.; Jing, T.; Zhong, W. A generalizable strategy for constructing ultralight three-dimensional hierarchical network heterostructure as high-efficient microwave absorber. *J. Colloid Interface Sci.* **2022**, *605*, 13–22. [[CrossRef](#)]
8. Liang, L.; Han, G.; Li, Y.; Zhao, B.; Zhou, B.; Feng, Y.; Ma, J.; Wang, Y.; Zhang, R.; Liu, C. Promising Ti3C2Tx MXene/Ni chain hybrid with excellent electromagnetic wave absorption and shielding capacity. *ACS Appl. Mater. Interfaces* **2019**, *11*, 25399–25409. [[CrossRef](#)]
9. Yang, F.; Yao, J.; Jin, L.; Huyan, W.; Zhou, J.; Yao, Z.; Liu, P.; Tao, X. Multifunctional Ti3C2Tx MXene/Aramid nanofiber/Polyimide aerogels with efficient thermal insulation and tunable electromagnetic wave absorption performance under thermal environment. *Compos. Part B Eng.* **2022**, *243*, 110161. [[CrossRef](#)]
10. Chen, X.; Liu, H.; Zheng, Y.; Zhai, Y.; Liu, X.; Liu, C.; Mi, L.; Guo, Z.; Shen, C. Highly Compressible and Robust Polyimide/Carbon Nanotube Composite Aerogel for High-Performance Wearable Pressure Sensor. *ACS Appl. Mater. Interfaces* **2019**, *11*, 42594–42606. [[CrossRef](#)]
11. Zhang, Q.; Chen, B.; Wu, K.; Nan, B.; Lu, M.; Lu, M. PEG-filled kapok fiber/sodium alginate aerogel loaded phase change composite material with high thermal conductivity and excellent shape stability. *Compos. Part A Appl. Sci. Manuf.* **2021**, *143*, 106279. [[CrossRef](#)]
12. Ahankari, S.; Paliwal, P.; Subhedar, A.; Kargarzadeh, H. Recent Developments in Nanocellulose-Based Aerogels in Thermal Applications: A Review. *ACS Nano* **2021**, *15*, 3849–3874. [[CrossRef](#)] [[PubMed](#)]
13. Zhang, C.; Huang, R.; Wang, P.; Wang, Y.; Zhou, Z.; Zhang, H.; Wu, Z.; Li, L. Highly Compressible, Thermally Conductive, yet Electrically Insulating Fluorinated Graphene Aerogel. *ACS Appl. Mater. Interfaces* **2020**, *12*, 58170–58178. [[CrossRef](#)] [[PubMed](#)]
14. Yang, J.; Tang, L.-S.; Bao, R.-Y.; Bai, L.; Liu, Z.-Y.; Yang, W.; Xie, B.-H.; Yang, M.-B. Largely enhanced thermal conductivity of poly(ethylene glycol)/boron nitride composite phase change materials for solar-thermal-electric energy conversion and storage with very low content of graphene nanoplatelets. *Chem. Eng. J.* **2017**, *315*, 481–490. [[CrossRef](#)]
15. Lv, P.; Miao, H.; Ji, C.; Wei, W. Highly compressible graphene aerogel with high thermal conductivity along both in-plane and through-plane directions. *Mater. Res. Express* **2021**, *8*, 045608. [[CrossRef](#)]
16. Gogotsi, Y.; Anasori, B. The Rise of MXenes. *ACS Nano* **2019**, *13*, 8491–8494. [[CrossRef](#)]
17. Kang, R.; Zhang, Z.; Guo, L.; Cui, J.; Chen, Y.; Hou, X.; Wang, B.; Lin, C.T.; Jiang, N.; Yu, J. Enhanced Thermal Conductivity of Epoxy Composites Filled with 2D Transition Metal Carbides (MXenes) with Ultralow Loading. *Sci. Rep.* **2019**, *9*, 9135. [[CrossRef](#)]

18. Liu, H.; Huang, Z.; Chen, T.; Su, X.; Liu, Y.; Fu, R. Construction of 3D MXene/Silver nanowires aerogels reinforced polymer composites for extraordinary electromagnetic interference shielding and thermal conductivity. *Chem. Eng. J.* **2022**, *427*, 131540. [[CrossRef](#)]
19. Kim, S.E.; Mujid, F.; Rai, A.; Eriksson, F.; Suh, J.; Poddar, P.; Ray, A.; Park, C.; Fransson, E.; Zhong, Y.; et al. Extremely anisotropic van der Waals thermal conductors. *Nature* **2021**, *597*, 660–665. [[CrossRef](#)]
20. Sood, A.; Xiong, F.; Chen, S.; Wang, H.; Selli, D.; Zhang, J.; McClellan, C.J.; Sun, J.; Donadio, D.; Cui, Y. An electrochemical thermal transistor. *Nat. Commun.* **2018**, *9*, 4510. [[CrossRef](#)]
21. Zhang, X.; Yeung, K.K.; Gao, Z.; Li, J.; Sun, H.; Xu, H.; Zhang, K.; Zhang, M.; Chen, Z.; Yuen, M.M. Exceptional thermal interface properties of a three-dimensional graphene foam. *Carbon* **2014**, *66*, 201–209. [[CrossRef](#)]
22. Qin, M.; Xu, Y.; Cao, R.; Feng, W.; Chen, L. Efficiently controlling the 3D thermal conductivity of a polymer nanocomposite via a hyperelastic double-continuous network of graphene and sponge. *Adv. Funct. Mater.* **2018**, *28*, 1805053. [[CrossRef](#)]
23. Wang, Q.; Xiang, L.; Mei, D.; Xie, Y. Graphene aerogels: Structure control, thermal characterization and thermal transport. *Int. J. Thermophys.* **2020**, *41*, 155. [[CrossRef](#)]
24. Du, T.; Xiong, Z.; Delgado, L.; Liao, W.; Peoples, J.; Kantharaj, R.; Chowdhury, P.R.; Marconnet, A.; Ruan, X. Wide range continuously tunable and fast thermal switching based on compressible graphene composite foams. *Nat. Commun.* **2021**, *12*, 4915. [[CrossRef](#)]
25. Pan, C.; He, P.; Wu, J.; Chen, N.; Wei, J.; Xu, T.; Shi, E.; Wang, A.; Jia, H. Copper foam effectively improves the thermal performance of graphene-aerogel composite phase-change materials for thermal storage. *J. Energy Storage* **2022**, *51*, 104485. [[CrossRef](#)]
26. Butt, H.A.; Owais, M.; Sulimov, A.; Ostrizhiniy, D.; Lomov, S.V.; Akhatov, I.S.; Abaimov, S.G.; Popov, Y.A. CNT/Epoxy-Masterbatch Based Nanocomposites: Thermal and Electrical Properties. In Proceedings of the 2021 IEEE 21st International Conference on Nanotechnology (NANO), Montreal, QC, Canada, 28–30 July 2021; pp. 417–420. [[CrossRef](#)]
27. Lee Sanchez, W.A.; Huang, C.Y.; Chen, J.X.; Soong, Y.C.; Chan, Y.N.; Chiou, K.C.; Lee, T.M.; Cheng, C.C.; Chiu, C.W. Enhanced Thermal Conductivity of Epoxy Composites Filled with Al<sub>2</sub>O<sub>3</sub>/Boron Nitride Hybrids for Underfill Encapsulation Materials. *Polymers* **2021**, *13*, 147. [[CrossRef](#)]
28. Zheng, X.; Kim, S.; Park, C.W. Enhancement of thermal conductivity of carbon fiber-reinforced polymer composite with copper and boron nitride particles. *Compos. Part A Appl. Sci. Manuf.* **2019**, *121*, 449–456. [[CrossRef](#)]
29. Nobile, M.R.; Raimondo, M.; Naddeo, C.; Guadagno, L. Rheological and Morphological Properties of Non-Covalently Functionalized Graphene-Based Structural Epoxy Resins with Intrinsic Electrical Conductivity and Thermal Stability. *Nanomaterials* **2020**, *10*, 1310. [[CrossRef](#)]
30. Song, S.H.; Park, K.H.; Kim, B.H.; Choi, Y.W.; Jun, G.H.; Lee, D.J.; Kong, B.S.; Paik, K.W.; Jeon, S. Enhanced thermal conductivity of epoxy-graphene composites by using non-oxidized graphene flakes with non-covalent functionalization. *Adv. Mater.* **2013**, *25*, 732–737. [[CrossRef](#)]
31. Kuang, Z.; Chen, Y.; Lu, Y.; Liu, L.; Hu, S.; Wen, S.; Mao, Y.; Zhang, L. Fabrication of highly oriented hexagonal boron nitride nanosheet/elastomer nanocomposites with high thermal conductivity. *Small* **2015**, *11*, 1655–1659. [[CrossRef](#)]
32. Lin, Z.; Liu, Y.; Raghavan, S.; Moon, K.-S.; Sitaraman, S.K.; Wong, C.-P. Magnetic alignment of hexagonal boron nitride platelets in polymer matrix: Toward high performance anisotropic polymer composites for electronic encapsulation. *ACS Appl. Mater. Interfaces* **2013**, *5*, 7633–7640. [[CrossRef](#)] [[PubMed](#)]
33. Zhi, C.; Bando, Y.; Terao, T.; Tang, C.; Kuwahara, H.; Golberg, D. Towards thermoconductive, electrically insulating polymeric composites with boron nitride nanotubes as fillers. *Adv. Funct. Mater.* **2009**, *19*, 1857–1862. [[CrossRef](#)]
34. Sun, H.; Xu, Z.; Gao, C. Multifunctional, ultra-flyweight, synergistically assembled carbon aerogels. *Adv. Mater.* **2013**, *25*, 2554–2560. [[CrossRef](#)]
35. Wu, Y.; Yi, N.; Huang, L.; Zhang, T.; Fang, S.; Chang, H.; Li, N.; Oh, J.; Lee, J.A.; Kozlov, M. Three-dimensionally bonded spongy graphene material with super compressive elasticity and near-zero Poisson's ratio. *Nat. Commun.* **2015**, *6*, 6141. [[CrossRef](#)] [[PubMed](#)]
36. Zhang, W.; Kong, Q.Q.; Tao, Z.; Wei, J.; Xie, L.; Cui, X.; Chen, C.M. 3D Thermally Cross-Linked Graphene Aerogel-Enhanced Silicone Rubber Elastomer as Thermal Interface Material. *Adv. Mater. Interfaces* **2019**, *6*, 1900147. [[CrossRef](#)]
37. Qiu, L.; Liu, J.Z.; Chang, S.L.; Wu, Y.; Li, D. Biomimetic superelastic graphene-based cellular monoliths. *Nat. Commun.* **2012**, *3*, 1241. [[CrossRef](#)]
38. Owais, M.; Shiverskii, A.; Sulimov, A.; Ostrizhiniy, D.; Popov, Y.; Mahato, B.; Abaimov, S.G. Scalable Fabrication of Thermally Conductive Layered Nacre-like Self-Assembled 3D BN-Based PVA Aerogel Framework Nanocomposites. *Polymers* **2022**, *14*, 3316. [[CrossRef](#)]
39. Yao, B.; Chen, J.; Huang, L.; Zhou, Q.; Shi, G. Base-Induced Liquid Crystals of Graphene Oxide for Preparing Elastic Graphene Foams with Long-Range Ordered Microstructures. *Adv. Mater.* **2016**, *28*, 1623–1629. [[CrossRef](#)]
40. An, F.; Li, X.; Min, P.; Liu, P.; Jiang, Z.G.; Yu, Z.Z. Vertically Aligned High-Quality Graphene Foams for Anisotropically Conductive Polymer Composites with Ultrahigh Through-Plane Thermal Conductivities. *ACS Appl. Mater. Interfaces* **2018**, *10*, 17383–17392. [[CrossRef](#)]
41. Ma, Y.; Chen, Y. Three-dimensional graphene networks: Synthesis, properties and applications. *Natl. Sci. Rev.* **2015**, *2*, 40–53. [[CrossRef](#)]

42. Zhao, Y.-H.; Wu, Z.-K.; Bai, S.-L. Study on thermal properties of graphene foam/graphene sheets filled polymer composites. *Compos. Part A Appl. Sci. Manuf.* **2015**, *72*, 200–206. [[CrossRef](#)]
43. Zhang, Q.; Xu, X.; Li, H.; Xiong, G.; Hu, H.; Fisher, T.S. Mechanically robust honeycomb graphene aerogel multifunctional polymer composites. *Carbon* **2015**, *93*, 659–670. [[CrossRef](#)]
44. Yang, X.; Fan, S.; Li, Y.; Guo, Y.; Li, Y.; Ruan, K.; Zhang, S.; Zhang, J.; Kong, J.; Gu, J. Synchronously improved electromagnetic interference shielding and thermal conductivity for epoxy nanocomposites by constructing 3D copper nanowires/thermally annealed graphene aerogel framework. *Compos. Part A Appl. Sci. Manuf.* **2020**, *128*, 105670. [[CrossRef](#)]
45. Yang, J.; Li, X.; Han, S.; Yang, R.; Min, P.; Yu, Z.-Z. High-quality graphene aerogels for thermally conductive phase change composites with excellent shape stability. *J. Mater. Chem. A* **2018**, *6*, 5880–5886. [[CrossRef](#)]
46. Min, P.; Liu, J.; Li, X.; An, F.; Liu, P.; Shen, Y.; Koratkar, N.; Yu, Z.-Z. Thermally Conductive Phase Change Composites Featuring Anisotropic Graphene Aerogels for Real-Time and Fast-Charging Solar-Thermal Energy Conversion. *Adv. Funct. Mater.* **2018**, *28*, 1805365. [[CrossRef](#)]
47. Liu, Z.; Wang, Q.; Hou, L.; Liu, Y.; Li, Z. Ultralight, Ultraflexible, Anisotropic, Highly Thermally Conductive Graphene Aerogel Films. *Molecules* **2021**, *26*, 6867. [[CrossRef](#)]
48. Liu, P.; Li, X.; Min, P.; Chang, X.; Shu, C.; Ding, Y.; Yu, Z.Z. 3D Lamellar-Structured Graphene Aerogels for Thermal Interface Composites with High Through-Plane Thermal Conductivity and Fracture Toughness. *Nano-Micro Lett.* **2020**, *13*, 22. [[CrossRef](#)]
49. Li, X.-H.; Liu, P.; Li, X.; An, F.; Min, P.; Liao, K.-N.; Yu, Z.-Z. Vertically aligned, ultralight and highly compressive all-graphitized graphene aerogels for highly thermally conductive polymer composites. *Carbon* **2018**, *140*, 624–633. [[CrossRef](#)]
50. Fang, H.; Zhao, Y.; Zhang, Y.; Ren, Y.; Bai, S.-L. Three-Dimensional Graphene Foam-Filled Elastomer Composites with High Thermal and Mechanical Properties. *ACS Appl. Mater. Interfaces* **2017**, *9*, 26447–26459. [[CrossRef](#)]
51. Conrado, F.; Pavese, M. A Continuous 3D-Graphene Network to Overcome Threshold Issues and Contact Resistance in Thermally Conductive Graphene Nanocomposites. *J. Nanomater.* **2017**, *2017*, 8974174. [[CrossRef](#)]
52. Weng, C.; Li, W.; Wu, J.; Shen, L.; Yang, W.; Deng, C.; Bao, N. Thermal shock exfoliated and siloxane cross-linked graphene framework for high performance epoxy-based thermally conductive composites. *J. Mater. Sci.* **2021**, *56*, 17601–17614. [[CrossRef](#)]
53. Shen, B.; Zhai, W.; Zheng, W. Ultrathin flexible graphene film: An excellent thermal conducting material with efficient EMI shielding. *Adv. Funct. Mater.* **2014**, *24*, 4542–4548. [[CrossRef](#)]
54. Ji, H.; Sellan, D.P.; Pettes, M.T.; Kong, X.; Ji, J.; Shi, L.; Ruoff, R.S. Enhanced thermal conductivity of phase change materials with ultrathin-graphite foams for thermal energy storage. *Energy Environ. Sci.* **2014**, *7*, 1185–1192. [[CrossRef](#)]
55. Yang, J.; Qi, G.-Q.; Liu, Y.; Bao, R.-Y.; Liu, Z.-Y.; Yang, W.; Xie, B.-H.; Yang, M.-B. Hybrid graphene aerogels/phase change material composites: Thermal conductivity, shape-stabilization and light-to-thermal energy storage. *Carbon* **2016**, *100*, 693–702. [[CrossRef](#)]
56. Renteria, J.D.; Ramirez, S.; Malekpour, H.; Alonso, B.; Centeno, A.; Zurutuza, A.; Cocemasov, A.I.; Nika, D.L.; Balandin, A.A. Strongly anisotropic thermal conductivity of free-standing reduced graphene oxide films annealed at high temperature. *Adv. Funct. Mater.* **2015**, *25*, 4664–4672. [[CrossRef](#)]
57. Cheng, Y.; Zhou, S.; Hu, P.; Zhao, G.; Li, Y.; Zhang, X.; Han, W. Enhanced mechanical, thermal, and electric properties of graphene aerogels via supercritical ethanol drying and high-temperature thermal reduction. *Sci. Rep.* **2017**, *7*, 1439. [[CrossRef](#)]
58. Chua, C.K.; Pumera, M. Chemical reduction of graphene oxide: A synthetic chemistry viewpoint. *Chem. Soc. Rev.* **2014**, *43*, 291–312. [[CrossRef](#)]
59. Xin, G.; Sun, H.; Scott, S.M.; Yao, T.; Lu, F.; Shao, D.; Hu, T.; Wang, G.; Ran, G.; Lian, J. Advanced phase change composite by thermally annealed defect-free graphene for thermal energy storage. *ACS Appl. Mater. Interfaces* **2014**, *6*, 15262–15271. [[CrossRef](#)]
60. Peng, L.; Xu, Z.; Liu, Z.; Guo, Y.; Li, P.; Gao, C. Ultrahigh thermal conductive yet superflexible graphene films. *Adv. Mater.* **2017**, *29*, 1700589. [[CrossRef](#)]
61. An, F.; Li, X.; Min, P.; Li, H.; Dai, Z.; Yu, Z.-Z. Highly anisotropic graphene/boron nitride hybrid aerogels with long-range ordered architecture and moderate density for highly thermally conductive composites. *Carbon* **2018**, *126*, 119–127. [[CrossRef](#)]
62. Yang, J.; Tang, L.-S.; Bao, R.-Y.; Bai, L.; Liu, Z.-Y.; Xie, B.-H.; Yang, M.-B.; Yang, W. Hybrid network structure of boron nitride and graphene oxide in shape-stabilized composite phase change materials with enhanced thermal conductivity and light-to-electric energy conversion capability. *Sol. Energy Mater. Sol. Cells* **2018**, *174*, 56–64. [[CrossRef](#)]
63. Zhang, C.; Huang, R.; Wang, Y.; Wu, Z.; Zhang, H.; Li, Y.; Wang, W.; Huang, C.; Li, L. Self-Assembled Boron Nitride Nanotube Reinforced Graphene Oxide Aerogels for Dielectric Nanocomposites with High Thermal Management Capability. *ACS Appl. Mater. Interfaces* **2020**, *12*, 1436–1443. [[CrossRef](#)]
64. Iijima, S. Helical microtubules of graphitic carbon. *Nature* **1991**, *354*, 56–58. [[CrossRef](#)]
65. Cao, Q.; He, F.; Xie, C.; Fan, J.; Wu, J.; Zhang, K.; Yang, Z.; Yang, W. Paraffin-based shape-stable phase change materials with graphene/carbon nanotube three-dimensional network structure. *Fuller. Nanotub. Carbon Nanostruct.* **2019**, *27*, 492–497. [[CrossRef](#)]
66. Kwon, Y.-K.; Kim, P. Unusually high thermal conductivity in carbon nanotubes. In *High Thermal Conductivity Materials*; Springer: Berlin/Heidelberg, Germany, 2006; pp. 227–265.
67. Xu, J.; Fisher, T.S. Enhancement of thermal interface materials with carbon nanotube arrays. *Int. J. Heat Mass Transf.* **2006**, *49*, 1658–1666. [[CrossRef](#)]
68. Zhang, Y.; Heo, Y.-J.; Son, Y.-R.; In, I.; An, K.-H.; Kim, B.-J.; Park, S.-J. Recent advanced thermal interfacial materials: A review of conducting mechanisms and parameters of carbon materials. *Carbon* **2019**, *142*, 445–460. [[CrossRef](#)]

69. Yao, Y.; Tey, J.N.; Li, Z.; Wei, J.; Bennett, K.; McNamara, A.; Joshi, Y.; Tan, R.L.S.; Ling, S.N.M.; Wong, C.-P. High-quality vertically aligned carbon nanotubes for applications as thermal interface materials. *IEEE Trans. Compon. Packag. Manuf. Technol.* **2014**, *4*, 232–239. [[CrossRef](#)]
70. Ivanov, I.; Puzek, A.; Eres, G.; Wang, H.; Pan, Z.; Cui, H.; Jin, R.; Howe, J.; Geohegan, D.B. Fast and highly anisotropic thermal transport through vertically aligned carbon nanotube arrays. *Appl. Phys. Lett.* **2006**, *89*, 223110. [[CrossRef](#)]
71. Lin, W.; Shang, J.; Gu, W.; Wong, C. Parametric study of intrinsic thermal transport in vertically aligned multi-walled carbon nanotubes using a laser flash technique. *Carbon* **2012**, *50*, 1591–1603. [[CrossRef](#)]
72. Hone, J.; Llaguno, M.; Nemes, N.; Johnson, A.; Fischer, J.; Walters, D.; Casavant, M.; Schmidt, J.; Smalley, R. Electrical and thermal transport properties of magnetically aligned single wall carbon nanotube films. *Appl. Phys. Lett.* **2000**, *77*, 666–668. [[CrossRef](#)]
73. Dong, Z.-J.; Sun, B.; Zhu, H.; Yuan, G.-M.; Li, B.-L.; Guo, J.-G.; Li, X.-K.; Cong, Y.; Zhang, J. A review of aligned carbon nanotube arrays and carbon/carbon composites: Fabrication, thermal conduction properties and applications in thermal management. *New Carbon Mater.* **2021**, *36*, 873–892. [[CrossRef](#)]
74. Zhang, X.; Li, X.; Yuan, G.; Dong, Z.; Ma, G.; Rand, B. Large diameter pitch-based graphite fiber reinforced unidirectional carbon/carbon composites with high thermal conductivity densified by chemical vapor infiltration. *Carbon* **2017**, *114*, 59–69. [[CrossRef](#)]
75. Golecki, I.; Xue, L.; Leung, R.; Walker, T.; Anderson, A.; Dewar, D.; Duncan, C.; Van Horik, J. Properties of high thermal conductivity carbon-carbon composites for thermal management applications. In Proceedings of the 1998 High-Temperature Electronic Materials, Devices and Sensors Conference (Cat. No. 98EX132), San Diego, CA, USA, 22–27 February 1998; pp. 190–195.
76. Wu, X.; Shi, S.; Wang, Y.; Tang, B.; Guo, L.; Gao, Y.; Jiang, T.; Yang, K.; Sun, K.; Zhao, Y.; et al. Polyethylene Glycol-Calcium Chloride Phase Change Materials with High Thermal Conductivity and Excellent Shape Stability by Introducing Three-Dimensional Carbon/Carbon Fiber Felt. *ACS Omega* **2021**, *6*, 33033–33045. [[CrossRef](#)] [[PubMed](#)]
77. Ma, X.; Wang, W.-Y.; Qi, X.-D.; Yang, J.-H.; Lei, Y.-Z.; Wang, Y. Highly thermally conductive epoxy composites with anti-friction performance achieved by carbon nanofibers assisted graphene nanoplatelets assembly. *Eur. Polym. J.* **2021**, *151*, 110443. [[CrossRef](#)]
78. Sheng, N.; Zhu, R.; Nomura, T.; Rao, Z.; Zhu, C.; Aoki, Y.; Habazaki, H.; Akiyama, T. Anisotropically enhanced heat transfer properties of phase change material reinforced by graphene-wrapped carbon fibers. *Sol. Energy Mater. Sol. Cells* **2020**, *206*, 110280. [[CrossRef](#)]
79. Yuan, G.; Li, X.; Dong, Z.; Xiong, X.; Rand, B.; Cui, Z.; Cong, Y.; Zhang, J.; Li, Y.; Zhang, Z. Pitch-based ribbon-shaped carbon-fiber-reinforced one-dimensional carbon/carbon composites with ultrahigh thermal conductivity. *Carbon* **2014**, *68*, 413–425. [[CrossRef](#)]
80. Lin, J.-F.; Yuan, G.-M.; Li, X.-K.; Dong, Z.-J.; Zhang, J.; Zhang, Z.-W.; Wang, J.-S. Preparation of 1D C/C composites with high thermal conductivity. *J. Inorg. Mater.* **2013**, *28*, 1338–1344. [[CrossRef](#)]
81. Yao, Y.-M.; Li, H.; Liu, Z.-Q. Microstructure and thermal conductivity of high thermal conductivity carbon/carbon composites. *J. Mater. Eng.* **2020**, *48*, 155–161.
82. Ding, J.-H.; Zhao, H.-R.; Yu, H.-B. High-yield synthesis of extremely high concentrated and few-layered boron nitride nanosheet dispersions. *2D Mater.* **2018**, *5*, 045015. [[CrossRef](#)]
83. Jiang, F.; Cui, S.; Rungnim, C.; Song, N.; Shi, L.; Ding, P. Control of a Dual-Cross-Linked Boron Nitride Framework and the Optimized Design of the Thermal Conductive Network for Its Thermoresponsive Polymeric Composites. *Chem. Mater.* **2019**, *31*, 7686–7695. [[CrossRef](#)]
84. Jing, L.; Li, H.; Tay, R.Y.; Sun, B.; Tsang, S.H.; Cometto, O.; Lin, J.; Teo, E.H.T.; Tok, A.I.Y. Biocompatible Hydroxylated Boron Nitride Nanosheets/Poly(vinyl alcohol) Interpenetrating Hydrogels with Enhanced Mechanical and Thermal Responses. *ACS Nano* **2017**, *11*, 3742–3751. [[CrossRef](#)]
85. Wu, W.; Liu, H.; Wang, Z.; Lv, P.; Hu, E.; Zheng, J.; Yu, K.; Wei, W. Formation of thermal conductive network in boron nitride/polyvinyl alcohol by ice-templated self-assembly. *Ceram. Int.* **2021**, *47*, 33926–33929. [[CrossRef](#)]
86. Song, P.; Liu, B.; Liang, C.; Ruan, K.; Qiu, H.; Ma, Z.; Guo, Y.; Gu, J. Lightweight, Flexible Cellulose-Derived Carbon Aerogel@Reduced Graphene Oxide/PDMS Composites with Outstanding EMI Shielding Performances and Excellent Thermal Conductivities. *Nano-Micro Lett.* **2021**, *13*, 91. [[CrossRef](#)] [[PubMed](#)]
87. Liu, Y.; Zhang, Y.; Liao, T.; Gao, L.; Wang, M.; Xu, X.; Yang, X.; Liu, H. Boron nitride-nanosheet enhanced cellulose nanofiber aerogel with excellent thermal management properties. *Carbohydr. Polym.* **2020**, *241*, 116425. [[CrossRef](#)]
88. Hu, J.; Huang, Y.; Yao, Y.; Pan, G.; Sun, J.; Zeng, X.; Sun, R.; Xu, J.B.; Song, B.; Wong, C.P. Polymer Composite with Improved Thermal Conductivity by Constructing a Hierarchically Ordered Three-Dimensional Interconnected Network of BN. *ACS Appl. Mater. Interfaces* **2017**, *9*, 13544–13553. [[CrossRef](#)] [[PubMed](#)]
89. Pan, D.; Dong, J.; Yang, G.; Su, F.; Chang, B.; Liu, C.; Zhu, Y.-C.; Guo, Z. Ice template method assists in obtaining carbonized cellulose/boron nitride aerogel with 3D spatial network structure to enhance the thermal conductivity and flame retardancy of epoxy-based composites. *Adv. Compos. Hybrid Mater.* **2021**, *5*, 58–70. [[CrossRef](#)]
90. Li, J.; Li, F.; Zhao, X.; Zhang, W.; Li, S.; Lu, Y.; Zhang, L. Jelly-Inspired Construction of the Three-Dimensional Interconnected BN Network for Lightweight, Thermally Conductive, and Electrically Insulating Rubber Composites. *ACS Appl. Electron. Mater.* **2020**, *2*, 1661–1669. [[CrossRef](#)]
91. Chen, J.; Huang, X.; Zhu, Y.; Jiang, P. Cellulose Nanofiber Supported 3D Interconnected BN Nanosheets for Epoxy Nanocomposites with Ultrahigh Thermal Management Capability. *Adv. Funct. Mater.* **2017**, *27*, 1604754. [[CrossRef](#)]

92. Bouville, F.; Deville, S. Dispersion of boron nitride powders in aqueous suspensions with cellulose. *J. Am. Ceram. Soc.* **2014**, *97*, 394–398. [[CrossRef](#)]
93. Kargar, F.; Barani, Z.; Salgado, R.; Debnath, B.; Lewis, J.S.; Aytan, E.; Lake, R.K.; Balandin, A.A. Thermal percolation threshold and thermal properties of composites with high loading of graphene and boron nitride fillers. *ACS Appl. Mater. Interfaces* **2018**, *10*, 37555–37565. [[CrossRef](#)]
94. Zhi, C.; Hanagata, N.; Bando, Y.; Golberg, D. Dispersible shortened boron nitride nanotubes with improved molecule-loading capacity. *Chem.–Asian J.* **2011**, *6*, 2530–2535. [[CrossRef](#)]
95. Gao, T.; Yang, Z.; Chen, C.; Li, Y.; Fu, K.; Dai, J.; Hitz, E.M.; Xie, H.; Liu, B.; Song, J. Three-dimensional printed thermal regulation textiles. *ACS Nano* **2017**, *11*, 11513–11520. [[CrossRef](#)] [[PubMed](#)]
96. Wang, Y.; Xu, N.; Li, D.; Zhu, J. Thermal properties of two dimensional layered materials. *Adv. Funct. Mater.* **2017**, *27*, 1604134. [[CrossRef](#)]
97. Fu, C.; Yan, C.; Ren, L.; Zeng, X.; Du, G.; Sun, R.; Xu, J.; Wong, C.-P. Improving thermal conductivity through welding boron nitride nanosheets onto silver nanowires via silver nanoparticles. *Compos. Sci. Technol.* **2019**, *177*, 118–126. [[CrossRef](#)]
98. Wang, J.; Liu, D.; Li, Q.; Chen, C.; Chen, Z.; Song, P.; Hao, J.; Li, Y.; Fakhrhoseini, S.; Naebe, M.; et al. Lightweight, Superelastic Yet Thermoconductive Boron Nitride Nanocomposite Aerogel for Thermal Energy Regulation. *ACS Nano* **2019**, *13*, 7860–7870. [[CrossRef](#)] [[PubMed](#)]
99. Li, Y.; Mehra, N.; Ji, T.; Yang, X.; Mu, L.; Gu, J.; Zhu, J. The stiffness–thermal conduction relationship at the composite interface: The effect of particle alignment on the long-range confinement of polymer chains monitored by scanning thermal microscopy. *Nanoscale* **2018**, *10*, 1695–1703. [[CrossRef](#)]
100. Du, X.; Qiu, J.; Deng, S.; Du, Z.; Cheng, X.; Wang, H. Alkylated Nanofibrillated Cellulose/Carbon Nanotubes Aerogels Supported Form-Stable Phase Change Composites with Improved n-Alkanes Loading Capacity and Thermal Conductivity. *ACS Appl. Mater. Interfaces* **2020**, *12*, 5695–5703. [[CrossRef](#)]
101. Wu, G.; Bing, N.; Li, Y.; Xie, H.; Yu, W. Three-dimensional directional cellulose-based carbon aerogels composite phase change materials with enhanced broadband absorption for light-thermal-electric conversion. *Energy Convers. Manag.* **2022**, *256*, 115361. [[CrossRef](#)]
102. Sun, K.; Kou, Y.; Dong, H.; Ye, S.; Zhao, D.; Liu, J.; Shi, Q. The design of phase change materials with carbon aerogel composites for multi-responsive thermal energy capture and storage. *J. Mater. Chem. A* **2021**, *9*, 1213–1220. [[CrossRef](#)]
103. Yue, J.; Pan, J.; Deng, Y.; Li, J.; Bao, J. Enhanced properties of poly (styrene-*b*-ethylene-co-butylene-*b*-styrene) nanocomposites with in situ construction of interconnected graphene network. *J. Appl. Polym. Sci.* **2019**, *136*, 47118. [[CrossRef](#)]
104. Wang, P.; Chong, H.; Zhang, J.; Lu, H. Constructing 3D graphene networks in polymer composites for significantly improved electrical and mechanical properties. *ACS Appl. Mater. Interfaces* **2017**, *9*, 22006–22017. [[CrossRef](#)] [[PubMed](#)]
105. Li, A.; Zhang, C.; Zhang, Y.-F. RGO/TPU composite with a segregated structure as thermal interface material. *Compos. Part A Appl. Sci. Manuf.* **2017**, *101*, 108–114. [[CrossRef](#)]
106. Alam, F.E.; Dai, W.; Yang, M.; Du, S.; Li, X.; Yu, J.; Jiang, N.; Lin, C.-T. In situ formation of a cellular graphene framework in thermoplastic composites leading to superior thermal conductivity. *J. Mater. Chem. A* **2017**, *5*, 6164–6169. [[CrossRef](#)]
107. Yang, L. Constructing of Highly Ordered 3D Network of Carbon Nanotube inside Polymer Matrix and the Improvements in Properties of the Composites. *Am. J. Polym. Sci. Technol.* **2019**, *5*, 9. [[CrossRef](#)]